Bone Reports 9 (2018) 181–187

Contents lists available at ScienceDirect

Bone Reports

journal homepage: www.elsevier.com/locate/bonr

Prevalence of glucocorticoid induced osteonecrosis in the mouse is not affected by treatments that maintain bone vascularity

Nancy E. Lane[a,*], Geetha Mohan[a], Wei Yao[a], Kie Shidara[a], Yu-An Evan Lay[a], Jia Junjing[b], Alanna Dubrovsky[a], Donald B. Kimmel[c]

[a] Center for Musculoskeletal Health, University of California at Davis Medical Center, Sacramento, CA 95817, USA
[b] Facility of Animal Science, Yunnan Agricultural University, Kunming, Yunnan, 650201, China
[c] Department of Physiological Sciences, University of Florida, Gainesville, FL 32610, USA

ARTICLE INFO

Keywords:
hPTH (1–34)
LLP2A-Ale
Distal femoral epiphysis
Dexamethasone
Prevention

ABSTRACT

Objective: Determine if LLP2A-Ale or PTH (1–34) affects the prevalence of glucocorticoid-induced osteonecrosis (ON) in a mouse model.

Methods: Eight-week-old young adult male BALB/cJ mice were weight-randomized into Control (Con), glucocorticoid (GC)-only, or concurrent treatments with GC and LLP2A-Ale (250 μg/kg or 500 μg/kg, IV, Days 1, 14, 28) or parathyroid hormone hPTH (1–34) (40 μg/kg, 5 ×/week). Mice were necropsied after 45 days for qualitative evaluation of prevalent ON and quantitative evaluation of vascularity in the distal femoral epiphysis (DFE); and quantitative evaluation of bone mass, microarchitecture, and strength in the distal femoral metaphysis and lumbar vertebral body.

Results: The prevalence of ON was 14% in the Con group and 36% in the GC-only group ($P = 0.07$). The prevalence of ON did not differ among GC-only, GC + LLP2A-Ale, and GC + PTH groups. GC-only mice had significantly lower trabecular and cortical bone strength than Con, while GC + LLP2A-Ale (500 μg/kg) and GC + PTH (1–34) groups had significantly greater trabecular bone strength than the GC-only group. GC + LLP2A-Ale (250 μg/kg and 500 μg/kg) and GC + PTH had significantly higher trabecular bone volume than GC-only mice at the vertebrae, distal femoral epiphyses and distal femoral metaphyses. DFE vascularity was lower in GC-only mice than in all other groups.

Conclusion: Neither LLP2A-Ale nor hPTH (1–34) reduced the prevalence of GC-induced ON, compared to GC-only mice. However, GC-treated mice given LLP2A-Ale or hPTH (1–34) had better bone mass, microarchitecture, and strength in trabecular-rich regions, and higher levels of vascularity than GC-only mice.

1. Introduction

Glucocorticoids (GCs) are used to treat rheumatoid arthritis, organ transplantation, dermatitis, asthma, systemic lupus erythematosis, and lymphoid malignancies. However, GCs appear to cause atraumatic femoral head osteonecrosis (ONFH) (Bouamar et al., 2009; Chan and Mok, 2012). Up to 40% of patients on long term GC therapy develop ONFH (Chan and Mok, 2012; Weinstein, 2010; Lane and Yao, 2010). Though the risk of ONFH increases with higher doses and longer use (Weinstein, 2012a; Weinstein, 2012b; Powell et al., 2010; Powell et al., 2011; Zhao et al., 2013), even short-term, low-dose GCs in steroid taper packs may induce ONFH (Dilisio, 2014). GCs reduce intraosseous circulation that eventually leads to ONFH and increased risk of femoral head collapse (Weinstein, 2012b; Glueck et al., 2001). In the US, the average age of diagnosis of GC-related ONFH is 35 years, with an annual incidence of 20,000–30,000, with 25–85% of those affected undergoing total hip arthroplasty (THA) within a few years of diagnosis, depending on the stage and extent of ON at diagnosis (Zalavras and Lieberman, 2014). In addition, GCs cause bone loss, reduce activation frequency of new bone remodeling units, and reduce osteoblast activity by lowering osteoblast lineage commitment to favor adipogenesis (Weinstein et al., 1998; Cui et al., 1997; Yao et al., 2008a).

Currently, there are no approved medications that slow the progression of early stage ONFH. Subjects with early stage ONFH usually report hip pain, a normal hip radiograph, and a hip MRI that demonstrates ONHF. Core decompression, the removal of a portion of the necrotic bone in the femoral head, stimulates new bone and blood vessel formation in the necrotic area and temporarily reduces hip pain

* Corresponding author at: Center for Musculoskeletal Health, U. C. Davis School of Medicine, 4625 Second Avenue, Suite 2006, Sacramento, CA 95918.
E-mail address: nelane@ucdavis.edu (N.E. Lane).

https://doi.org/10.1016/j.bonr.2018.10.003
Received 29 June 2018; Received in revised form 24 September 2018; Accepted 31 October 2018
Available online 03 November 2018

(Bednarek et al., 2010; Camp and Colwell, 1986; Wang et al., 1985). However, though it may delay, it rarely completely prevents further femoral head collapse, and THA is usually required (Classen et al., 2017). Randomized clinical trials report that alendronate reduces hip pain and delays femoral head collapse in early stage ONFH (Lai et al., 2005; Chen et al., 2012). Pre-clinical proof of concept studies of early stage ONFH with anti-platelet agents, statins, and autologous implantation of bone marrow–derived mesenchymal stem cells (MSCs) alone or combined with core decompression or scaffolds found that these treatments prevent the development or worsening of GC-related ONFH. Addition of autologous MSCs to core decompression reduced femoral head deterioration compared to core decompression alone by 80% after five years (Yamaguchi et al., 2012; Peng et al., 2011; Xie et al., 2012; Zhao et al., 2012). Evaluation of either scaffold or MSC-based therapies for ONFH found that the success of both required neovascularization to ensure sufficient perfusion of the necrotic area (Sheng et al., 2009; Cao et al., 2017).

LLP2A-Ale is a bone targeted agent that guides endogenous or exogenous mesenchymal stromal cells (MSCs) to bone (Peng et al., 2006; Yao and Lane, 2015; Guan et al., 2012), as alendronate has high affinity for bone and the LLP2A portion has high affinity for the α4β1 receptor that is present on MSCs. Previous studies have shown that LLP2A-Ale prevented bone loss induced by estrogen deficiency (Yao et al., 2013) and accelerated fracture healing (Yao et al., 2013; Yao et al., 2016a). Both LLP2A-Ale and PTH prevented GC-related bone loss in Swiss-Webster mice, associated with preservation of blood vessel density within the femur (Mohan et al., 2017). Parathyroid hormone [hPTH (1–34), teriparatide, TPTD) is a bone anabolic agent that is approved for treatment of severe osteoporosis (Neer et al., 2001). In patients with GC-induced osteoporosis (GIOP), TPTD (20 μg/d) increases bone mineral density (BMD) at the spine and hip and decreases risk of vertebral fracture more than alendronate (Saag et al., 2007; Saag et al., 2009). Human PTH (1–34) counteracts the adverse effects of GCs on osteoblast and osteocyte viability, bone formation, and bone strength (Weinstein et al., 2010; Yao et al., 2008b). Human PTH (1–34) also improves the effects of core decompression in an ONFH animal model, partially through revascularization (Zhou et al., 2017).

Since both LLP2A-Ale and hPTH (1–34) appear to improve bone vascularity in the presence of GCs (Mohan et al., 2017) in Swiss-Webster mice, a strain with low susceptibility to GC-related ON (Yang et al., 2009), the aim of this study was to use a young adult mouse model of GC-related ON (Kawedia et al., 2012; Janke et al., 2013; Liu et al., 2016; Yang et al., 2009) to evaluate the effects of LLP2A-Ale or PTH on: a) ON prevalence, b) vascularity, c) bone mass and microarchitecture, and d) bone strength.

2. Materials and methods

2.1. Animals, experimental design, and procedures

Eight-week-old young adult male BALB/cJ mice (Jackson Laboratory; Sacramento, *CA*. USA), a strain with high susceptibility to GC-induced ON of the distal femoral epiphysis (DFE) (Kawedia et al., 2012; Janke et al., 2013; Liu et al., 2016; Yang et al., 2009), were used. Other studies have determined males to be more susceptible to GC-induced ON than females (Weinstein et al., 2010; Ikemura et al., 2010). Body weight (BW) of each mouse was recorded weekly throughout the experiment. Mice were randomized into five groups based on initial BW: Control (fresh drinking water, $n = 8$); GC-only (dexamethasone (4 mg/L in drinking water; [Sigma-Aldrich; St. Louis, MO]; $n = 18$); GC + LLP2A-Ale (250 μg/kg intravenously in the tail vein, [Days 1, 14, and 28], $n = 13$); GC+ LLP2A-Ale (500 μg/kg IV, [Days 1, 14, and 28], $n = 15$); and GC + PTH (hPTH {1–34} (40 μg/kg subcutaneous injection, 5d/wk.; (Bachem Inc., Torrance, CA), $n = 14$). GC-only mice received no vehicle injections for either LLP2A-Ale or hPTH (1–34). LLP2A-Ale groups received no PTH vehicle injections and PTH groups received no LLP2A-Ale vehicle injections. Mice were housed singly in plastic cages, to avoid fighting-related wounds that heal poorly during GC treatment. The room had a 12:12-h dark:light cycle and a constant temperature range of 20–22 °C. Mice were fed commercial rodent chow (22/5 Rodent Diet 8640; Teklad; Madison, WI) with 0.95% calcium and 0.67% phosphorus *ad libitum*. All mice were euthanized by CO_2 asphyxiation after 45 days. At necropsy, both femurs were removed for histologic assessment of ON. MicroCT scanning was performed on the right distal femoral metaphysis and fifth lumbar vertebrae (LV5). Bone histomorphometric measurements were performed on the right DFE. The left tibiae and LV5 were disarticulated, cleaned of adherent muscle, wrapped in saline-soaked gauze and stored at −20 °C until bone strength testing. Immunohistochemical studies to identify the vasculature were performed on the right DFE.

These studies were carried out with strict adherence to recommendations in the Guide for the Care and Use of Laboratory Animals of the National Institutes of Health. All animals were treated according to the USDA animal care guidelines with the approval of the UC Davis Institutional Animal Care and Utilization Committee.

2.2. MicroCT (Right distal femoral metaphysis and LV5)

At necropsy, both femurs were fixed in 10% neutral-buffered formalin (NBF). After 48 h, the right femur was moved to 70% ethanol. The right distal femoral metaphysis (DFM) was then scanned with MicroCT (VivaCT 40, Scanco Medical AG, Bassersdorf, Switzerland) at 70 kev and 85 μA with an isotropic resolution of 10.5 μm in all three dimensions. Scanning was initiated distal to the level of the growth cartilage-metaphyseal junction and extended proximally for 250 slices. At the conclusion of scanning, the right femur was returned to 10% NBF. Scan evaluation was performed on a distal femoral metaphyseal trabecular bone volume of interest (VOI) that comprised 150 slices beginning 0.2 mm proximal to the most proximal point along the boundary of the growth cartilage with the metaphysis. LV5 was thawed, unwrapped, and scanned transversely in its entirety, then rewrapped and refrozen. LV5 scan evaluation was performed on a trabecular bone VOI in the body that excluded 25 slices at the cranial and caudal ends of the vertebral body. All trabecular bone in each marrow cavity was evaluated. For each slice, the VOI was defined as ~0.25 mm internal to the boundary of the marrow cavity with the cortex. The methods for calculating bone volume (BV), total volume (TV), trabecular thickness (Tb.Th), trabecular number (Tb.N), and structure model index (SMI) have been described (Bouxsein et al., 2010).

2.3. Histologic analysis of osteonecrosis

The distal 6 mm of each femur was then sawed free from the remainder of the femur with an Isomet bone saw (Buehler, Lake Bluff, Illinois), returned to 10% neutral buffered formalin, and then fully decalcified in 5% EDTA (pH 7.2). The specimens were then processed in ascending concentrations of ethanol and embedded in paraffin. Five μm thick parasagittal sections through the middle of each specimen were prepared, affixed to glass slides, stained with hematoxylin and eosin and evaluated for ON in the DFE as below.

Published criteria were used to define ON. They required one epiphyseal region containing 6–8 confluent, empty osteocyte lacunae in trabeculae surrounded by adipocytes and/or necrotic marrow stroma (Kawedia et al., 2012; Janke et al., 2013; Liu et al., 2016; Yang et al., 2009) (Fig. 1). Presence or absence of ON in each DFE was assessed from a randomly-ordered slide set that contained one section from each femur of each mouse per slide, by two histopathologists working independently (DK, WY) who were blinded to treatment group. A single complete, intact, well-fixed and stained section of a DFE was required for successful ON assessment (Fig. 1). The possible diagnoses for each DFE were: a) ON-positive; b) ON-free; and c) insufficient readable tissue to assign status. Acceptable readability required finding adequate

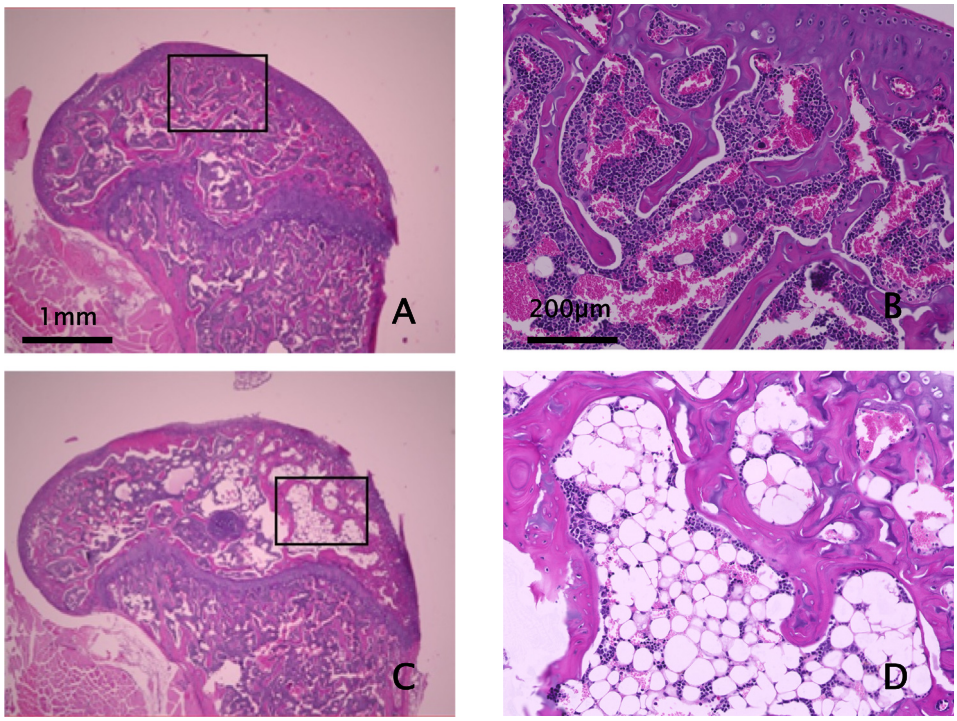

Fig. 1. Photomicrographs of Osteonecrosis-Free and Osteonecrosis-Positive Distal Femoral Epiphyses

A&B- Representative 5 µm thick H&E-stained parasagittal section of an ON-free distal femoral epiphysis. B is higher magnification photomicrograph of box in A. Note abundant hematopoietic marrow with occasional adipocytes and trabeculae with most osteocyte lacunae showing healthy nuclei. Occasional, isolated empty lacunae exist randomly in normal bone due to the relative size of lacunae, 5 µm section thickness, and positioning of nuclei in neighboring sections. Scale bars = 1 mm (A) and 200 µm (B).

C&D- Representative section from an ON-positive distal femoral epiphysis. D is higher magnification photomicrograph of box in C. A positive diagnosis of ON in a DFE required the presence of both fatty marrow or necrotic bone marrow stroma that surrounded trabeculae, and multiple confluent empty osteocyte lacunae (Kawedia et al., 2012; Janke et al., 2013; Liu et al., 2016; Yang et al., 2009). Most ON-positive DFE's had only a portion, occasionally as little as 10%, of the epiphysis involved with ON. Nonetheless, note copious amount of fatty marrow in D, with trabeculae containing multiple confluent empty lacunae. Fields with fatty marrow or stromal necrosis surrounding trabeculae that contained only lacunae with healthy osteocyte nuclei were not uncommon. Only when fat or marrow necrosis-enveloped trabeculae also had multiple confluent empty osteocyte lacunae was the specimen designated as ON-positive. Multiple confluent empty osteocyte lacunae in trabeculae were never observed in the midst of healthy, hematopoietic marrow. Scale bars as for A&B = 1 mm (C) and 200 µm (D).

fixation of the adjacent marrow and stroma before osteocyte lacunae of nearby bone tissue in question could be classified as empty or occupied. After the independent reading, the histopathologists reviewed together all DFEs in which their ON status assignments differed, and reached mutual agreement on the status of each DFE. Based on the agreed status of each DFE, the ON diagnosis of each *mouse* was determined as follows: a) when neither DFE had sufficient tissue, the mouse was discarded; b) when one DFE was ON-positive, regardless of the status of the other DFE, the mouse was considered ON-positive; c) when both DFEs had sufficient readable tissue and both were assigned ON-free status, the mouse was considered ON-free; and d) when one DFE was ON-free and the other DFE had insufficient tissue, the mouse was discarded.

2.4. Static bone histomorphometry (Right DFE)

Static bone histomorphometric measurements were performed using semi-automatic image analysis (Bioquant Image Analysis Corporation, Nashville, TN USA). The entire DFE trabecular bone region inside a boundary 25 µm inside its endocortical surface was evaluated. Data collected included total tissue area (Tt.Ar), trabecular bone area (B.Ar), and adipocyte tissue area (Ad.Ar). These data were used to calculate trabecular bone volume (BV/TV), trabecular number (Tb.N), trabecular thickness (Tb.Th), trabecular separation (Tb.Sp), and adipocyte volume (AV/TV) (Yao et al., 2016b; Dempster et al., 2013).

2.5. Bone strength

Bone strength was measured in the central left tibia by three-point bending and in LVB5 by compression testing (858 MiniBionix; MTS, Eden Prairie, MN, USA). Prior to testing, all specimens were thawed to room temperature and unwrapped from the gauze. The tibia was placed on two lower supports with an inter-support distance of 10 mm, with the tibial midpoint midway between the supports and the anterior surface facing up. The load was applied from above to the anterior surface at the tibial midpoint. Each tibia was irrigated constantly with 37 °C HBSS throughout the test and loaded to failure at a rate of 0.1 mm/s while the load-displacement curve was recorded electronically using a calibrated 1 kN load cell. The values for maximum load and work to failure were determined from the load-displacement curve by manufacturer's software (Yao et al., 2016a; Yao et al., 2016b).

Bone strength of LVB5 was measured in compression. Transverse and posterior processes were removed with an Isomet bone saw (Buehler Co., Lake Bluff, IL USA). The cartilaginous endplates were removed with the Isomet, leaving parallel faces on the cranial and caudal ends. The specimen was placed with the parallel faces between two smooth, lubricated platens (5 mm diameter), and displacement was measured across the platens. The LVB5 test specimen was loaded at 0.05 mm/s in compression. The load-displacement curve was recorded electronically and the value for maximum load was determined as above.

2.6. Immunohistochemistry

Five micron thick paraffin sections of the right DFE were selected randomly from four mice of each group. Endothelial biomarkers were evaluated by labeling sections with antibodies to Endomucin (1:50, Abcam, ab106100, Cambridge, MA) (Fig. 3A) and CD31 (1:50, Abcam, ab28364, Cambridge, MA USA) (Fig. 3B). Secondary antibodies included Donkey Anti-Rabbit IgG H&L (1:500, Alexa Fluor® 647, ab150075, Cambridge, MA USA) and Donkey Anti-Rat IgG H&L (1:500, Alexa Fluor® 488, ab150153, Cambridge, MA USA). Sections were washed in PBS and incubated in 0.3% H_2O_2 for 5 min to quench endogenous peroxidase activity. Then the sections were washed in PBS and incubated with a blocking reagent (1% bovine serum albumin) for 60 min. The blocking reagent was removed, and the sections were incubated overnight in primary antibodies. The sections were washed with PBS and incubated with appropriate Alexa Fluor-coupled secondary antibodies for 2 h, protected from light. Sections were thoroughly washed with PBS and mounted using ProLong® Gold antifade reagent with DAPI (Molecular Probes, P36935, Eugene, OR USA).

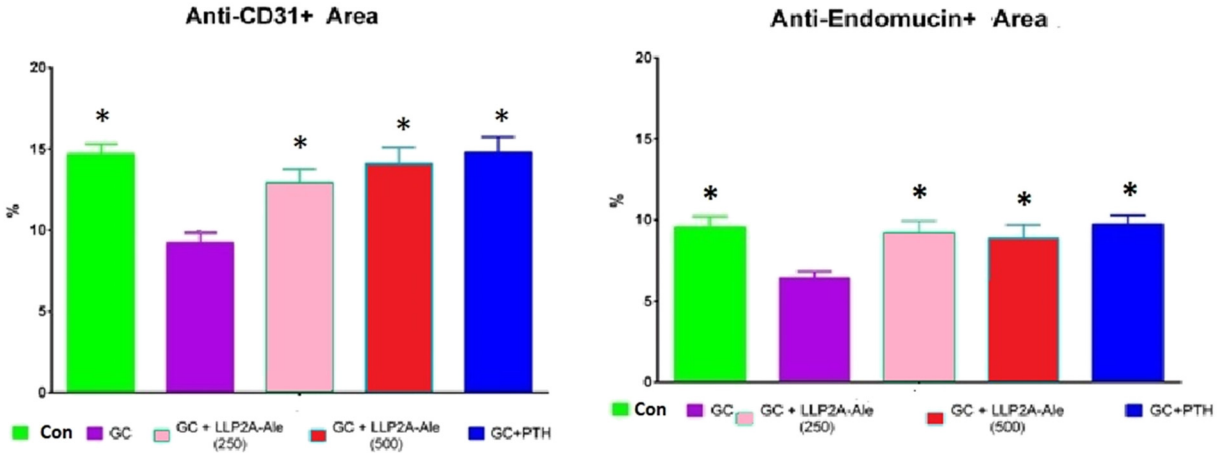

Fig. 2. Immunofluorescence Labeled Percent Area for CD31/PECAM1 and Endomucin in the Distal Femoral Epiphysis
A) % of CD31+ Cells; Mean ± SEM; *Compared to GC-only ($p < 0.05$).
B) % of Endomucin+ Cells; Mean ± SEM; *Compared to GC-only ($p < 0.05$).

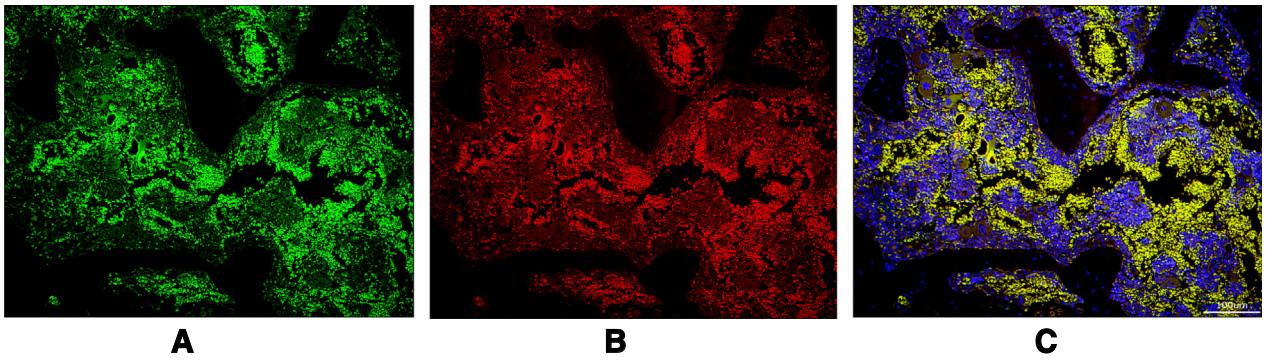

Fig. 3. Immunofluorescence Labeling for CD31/PECAM1 and Endomucin of same Region in the Distal Femoral Epiphysis
A) Representative photomicrograph of immunofluorescence labeling for CD31/PECAM1. Scale bar (100 μm) in lower right corner of Fig. 3C applies.
B) Representative photomicrograph of immunofluorescence labeling for Endomucin. Scale bar (100 μm) in lower right corner of Fig. 3C applies.
C) Representative photomicrograph of immunofluorescence labeling for merged CD31/PECAM1 and Endomucin. Scale bar (100 μm) in lower right corner.

Immunohistochemically-labeled sections were evaluated by microscopy (Biorevo BZ-9000, Keyence, Osaka, Japan). The DFE was evaluated for labeling percent area using a BZ-II Analyzer (Keyence, Osaka, Japan). The percentage reflects the total area of positive cells (pixel intensity > 100) in the DFE (Yao et al., 2016a; Zhang et al., 2017) (Figs. 2 and 3).

2.7. Statistical analysis

The group means and standard deviations were calculated for all variables. Non-parametric Kruskal-Wallis ANOVA was first applied for continuous variables. If significance was detected, non-parametric Dunn's multiple comparison post-hoc tests were used to determine differences only with respect to the GC group. For dichotomous outcomes (presence/absence of ON), we used Fisher's Exact Text. Differences were considered significant at $p < 0.05$.

3. Results

3.1. Body weight and well-being (Table 2)

Initial body weight did not differ among the groups. However, at the end, Control mice weighed significantly more than all other groups. There was no significant difference among the GC-treated groups.Eleven mice (16%) died on study (Control (n = 1), GC-only (n = 3); GC+LLP2A-Ale 250 (n = 1), GC+LLP2A-Ale 500 (n = 2), and GC + PTH (n = 4)). This loss rate is consistent with previous experiments with this model (Kawedia et al., 2012; Janke et al., 2013; Liu et al., 2016; Yang et al., 2009).

3.2. Osteonecrosis prevalence (Table 1)

Photomicrographs of ON-free and ON-positive distal femoral epiphyses are shown (Fig. 1). The prevalence of ON was 14% in the Control group and 36% in the GC-only group ($P < 0.05$). ON prevalence did not differ among GC-only, GC + LLP2A-Ale, and GC + PTH groups.

3.3. Static histomorphometry (Distal femoral epiphysis) (Table 2)

GC-only mice had lower bone volume, trabecular thickness, and trabecular number than Control mice. GC + LLP2A-Ale 250 mice had

Table 1
Osteonecrosis prevalence (%) by group.

Group	ON+	ON-free	Discard	Final	ON%
Control	1	6	0	1/7	14
GC-only	5	9	1	5/14	36
GC + LLPA-250	2	9	2	2/11	18
GC + LLPA-500	4	9	1	4/13	31
GC + PTH	3	7	1	3/10	30

Table 2
Bone mass, microarchitecture, and strength of femur, lumbar vertebral body and tibia.

Group		Control		GC-only		GC + LLP250		GC + LLP500		GC + PTH
Variable (Mean ± SD)	N		N		N		N		N	
Body weight										
Initial (g)	7	24.8 ± 1.9	14	25.6 ± 2.2	11	25.9 ± 1.2	13	25.4 ± 1.2	10	25.4 ± 0.9
Final (g)	7	28.9 ± 1.1[b]	14	25.4 ± 1.7	10	24.9 ± 1.5	13	24.6 ± 1.5	10	25.4 ± 1.6
Distal femoral epiphysis bone mass and microarchitecture										
Bone volume	7	0.371 ± 0.109[b]	15	0.241 ± 0.059	7	0.196 ± 0.034[b]	8	0.286 ± 0.058	8	0.304 ± 0.074[b]
Trabecular number (mm^{-1})	7	6.74 ± 1.61[b]	15	9.92 ± 1.75	7	10.37 ± 1.21	8	9.44 ± 1.22	8	10.05 ± 1.57
Trabecular thickness (μm)	7	108.7 ± 39.7[b]	15	58.1 ± 17.5	7	49.0 ± 10.1	8	64.3 ± 8.7	8	64.2 ± 20.7
Trabecular spacing (μm)	7	47.2 ± 10.2	15	46.3 ± 8.1	7	48.7 ± 3.1	8	43.1 ± 9.3	8	38.0 ± 4.0[b]
Adipocyte volume	7	0.36 ± 0.24[b]	14	2.17 ± 1.71	12	1.16 ± 089[b]	13	2.60 ± 3.95	9	1.91 ± 2.01
Distal femoral metaphysis bone mass and microarchitecture										
Bone volume	7	0.205 ± 0.011	15	0.189 ± 0.019	11	0.209 ± 0.029[b]	13	0.213 ± 0.020[b]	10	0.251 ± 0.033[b]
Trabecular number (mm^{-1})	7	4.42 ± 0.31	15	4.54 ± 0.24	11	4.72 ± 0.21	13	4.63 ± 0.32	10	4.87 ± 0.23[b]
Trabecular thickness (μm)	7	46.94 ± 1.19[b]	15	43.68 ± 1.89	11	45.26 ± 2.52[b]	13	45.95 ± 2.27[b]	10	50.32 ± 3.19[b]
Trabecular spacing (μm)	7	231 ± 18	15	223 ± 12	11	214 ± 10	13	220 ± 17	10	209 ± 11[b]
Structure-model index	7	0.804 ± 0.160[b]	15	1.054 ± 0.218	11	0.900 ± 0.332	13	0.875 ± 0.192[b]	10	0.474 ± 0.303[b]
LVB5 bone mass and microarchitecture										
Bone volume	7	0.205 ± 0.011	15	0.189 ± 0.019	9	0.212 ± 0.032[b]	13	0.213 ± 0.020[b]	9	0.245 ± 0.028[b]
Trabecular number (mm^{-1})	7	4.91 ± 0.22	15	4.85 ± 0.33	9	5.20 ± 0.36[b]	13	5.23 ± 0.29[b]	9	5.29 ± 0.28[b]
Trabecular thickness (μm)	7	41.6 ± 0.9[b]	15	38.5 ± 2.3	9	40.3 ± 3.7	13	40.5 ± 2.4[b]	9	46.3 ± 3.3[b]
Trabecular spacing (μm)	7	162 ± 9	15	169 ± 17	9	153 ± 17[b]	13	151 ± 12[b]	9	143 ± 12[bc]
Bone strength										
LVB Ultimate Load (N)	6	52.9 ± 7.9[b]	15	35.8 ± 9.9	9	42.8 ± 10.2	13	45.3 ± 10.0[b]	10	44.0 ± 8.2[b]
CT ultimate load (N)	7	16.64 ± 1.74[b]	15	13.15 ± 1.00	12	13.81 ± 1.44	14	13.73 ± 1.44	10	13.64 ± 1.40
CT work to failure (N-mm)	7	4.68 ± 1.67[b]	15	3.19 ± 0.96	12	3.17 ± 0.96	14	3.39 ± 1.07	10	3.60 ± 1.06

GC-glucocorticoid; LVB- lumbar vertebral body; CT- Central Tibia.
[b] diff from GC-only ($P < 0.05$).

lower bone volume and GC + PTH mice had higher bone volume, than GC-only mice ($P < 0.05$). Trabecular spacing was significantly lower in GC + PTH mice than in GC-only mice ($P < 0.05$). GC-only mice had significantly higher adipocyte volume than control mice ($P < 0.05$). LLP2A-Ale 250 mice had lower adipocyte volume than GC-only mice ($P < 0.05$).

3.4. Bone mass and microarchitecture (MicroCT)

3.4.1. Distal femoral metaphysis (Table 2)

Bone volume in GC-only and control mice did not differ. However, trabecular thickness was significantly less and structure-model index was significantly greater in GC-only mice than in Control mice. Bone volume was significantly greater in GC + LLP2A-Ale 250, GC + LLP2A-Ale 500, and GC + PTH mice than in GC-only mice. Trabecular number was significantly greater in GC + PTH mice than in GC-only mice. However, trabecular thickness in GC + LLP2A-Ale 250, GC + LLP2A-Ale 500, and GC + PTH was greater and structure-model index was significantly less in GC + LLP2A-Ale 500 and GC + PTH mice, than in GC-only mice. Trabecular spacing was significantly less in GC + PTH mice than in GC-only mice.

3.4.2. Lumbar vertebral body 5 (Table 2)

Bone volume and trabecular number in GC-only and control mice did not differ. However, trabecular thickness was significantly less in GC-only mice than in Control mice. Bone volume and trabecular number were significantly greater and trabecular spacing was significantly less in GC + LLP2A-Ale 250, GC + LLP2A-Ale 500, and GC + PTH mice than in GC-only mice. Trabecular thickness was also significantly greater in GC + LLP2A-Ale 500 and GC + PTH mice than in GC-only mice.

3.4.3. Bone strength (Table 2)

Ultimate load in both the central tibia and LVB5 and work to failure of the central tibia were significantly lower in GC-only mice than in Control mice ($P < 0.05$). Ultimate load of LVB5 was significantly higher in GC + LLP2A-Ale 500 and GC + PTH mice than in GC-only mice ($P < 0.05$). However, ultimate load and work to failure of the central tibia did not differ from GC-only mice with any treatment.

3.4.4. Immunohistochemistry (Fig. 2)

The percentage area of CD31 and Endomucin labeling was lower in GC-only mice than in Control mice, and was greater in all treatment groups than in GC-only mice.

4. Discussion

ON is an adverse event in patients treated with GCs (Weinstein, 2012a). Based on our earlier report that GCs reduced vascular density in the mouse femur (Mohan et al., 2017), this study evaluated if two bone active agents, LLP2A-Ale and hPTH (1–34), that preserve bone vascularity in the presence of GCs, reduce prevalent GC-induced ON of the distal femoral epiphysis (DFE). GC-only mice had a 36% prevalence of ON. Concurrent treatment of GC-treated mice with hPTH (1–34) and LLP2A-Ale did not change the rate of prevalent ON. The higher prevalence of ON in GC-only mice than in control mice was associated with reduced vascularity, lower trabecular bone mass, increased adipocyte volume within the bone marrow of the DFE and lower trabecular and cortical bone strength. While a quantitative assessment indicated that GC + LLP2A-Ale and GC + hPTH (1–34) groups maintained vascularity at control levels, prevalent ON after treatment with those agents was not different from GC-only treatment.

Our study confirmed that the DFE of the young adult male Balb/cJ mouse is susceptible to the development of ON (Kawedia et al., 2012; Janke et al., 2013; Liu et al., 2016; Yang et al., 2009). Indeed, we observed one ON case in control mice, suggesting the possibility that GCs interact with a metabolic or structural characteristic of the DFE that raises the intrinsic risk of ON in Balb/cJ mice, to cause GC-related ON. Previous investigators screened fourteen strains of mice for the development of GC-induced ON (Yang et al., 2009), determining a 40%

prevalence of DFE ON in male BALB/cJ mice treated with dexamethasone for 12 weeks. Our data confirmed a similar prevalence in GC-only mice after six weeks, providing multi-laboratory validation for this model.

Recently, the development of GC-induced ON in the femoral head of male C57BL/6 mice treated for 42 days with an implanted slow release prednisolone pellet was confirmed (Weinstein, 2012a; Weinstein, 2012b; Weinstein et al., 2017). At day 14, GC mice showed increased osteoclast number in the femoral head, and reduced VEGF, Hif-1α, osteoblast number, bone formation, and bone strength with no difference in bone density when compared to either baseline or concurrent control mice. However, at Day 28, lower bone mass and strength, deteriorated microarchitecture, and both histologic and MRI evidence of ON was present (Weinstein et al., 2017). Therefore, assessment of GC-related ON can be done in both Balb/cJ and C57BL/6 male mice, when appropriate sites are investigated.

Our histologic findings of GC-induced ON are consistent with other reports that the lesions have low trabecular bone volume, increased adipocyte numbers, and reduced blood vessel volume (Kawedia et al., 2012; Janke et al., 2013; Liu et al., 2016; Yang et al., 2009). However, concurrent treatment with either LLP2A-Ale or hPTH (1–34), agents that preserved bone vascular density in the presence of GCs in both Swiss-Webster mice (Mohan et al., 2017) and Balb/cJ mice, did not reduce prevalent ON in Balb/cJ mice. Treatment of rats with established GC-induced ON with either hPTH (1–34) or vehicle showed ON incidence of 17% in the hPTH (1–34) group and 75% in the vehicle group after four weeks (Dong et al., 2015). The investigators hypothesized that hPTH (1–34) prevented ON by increasing MSC activity and osteogenic differentiation, thus reversing the effects of GCs on the ON repair process (Dong et al., 2015). Both LLP2A-Ale and PTH prevented GC-related bone loss in Swiss-Webster mice, associated with preservation of blood vessel density within the femur (Mohan et al., 2017). However, neither prevented ON in this Balb/cJ mouse model.

The lack of approved medications that slow the progression of early stage ONFH in humans tempers what can be formally learned from this and other pre-clinical ON medicinal treatment attempts. Without an approved medication for human ONFH to use as a standard, it is difficult to determine whether a pre-clinical ON treatment model consistently predicts human treatment outcomes. Though this mouse model of GC-related ON appears to recapitulate the development of ON in a reasonable fashion, it has seldom been used to test agents for their ability to prevent or treat ON (Kawedia et al., 2012; Janke et al., 2013; Liu et al., 2016; Yang et al., 2009). Since this experiment was done in prevention mode, it seems likely that two different phases of ON, initiation and progression, were addressed. Though these drugs appear to have affected neither phase, one might speculate that these agents that increased bone vascularity would be more likely to act in the progression phase by interfering with vascular collapse. Nonetheless, despite the outcome, the nascent nature of pre-clinical models of ON should cause one to hesitate at this time to conclude that agents that promote vascularity cannot influence ON.

This study has several strengths including the use of an established mouse model with a clear definition of ON (Kawedia et al., 2012; Janke et al., 2013; Liu et al., 2016; Yang et al., 2009) and quantitative assessments of vascularity, bone mass, microarchitecture, and strength. However, there were also some shortcomings. Our results are based on prevalence of early stage ON in which only histologic criteria are applied. This is quite different from human ON in which pain, clinical history, and abnormal radiographs and/or MRI scans are among the usual diagnostic criteria. Furthermore, it is not known if these mouse ON lesions will progress to late stage ON with the subchondral bone collapse and arthritis seen in humans. We used only male mice that may prevent generalization to females. We evaluated both DFEs for ON. Previous work suggests that proximal tibial epiphyseal ON can occur independently of that in the DFE, something that could increase ON prevalence in whole animals (Kawedia et al., 2012; Janke et al., 2013; Liu et al., 2016; Yang et al., 2009). In humans, the site with the highest prevalence of and greatest morbidity from ON is the femoral head. DFE osteonecrosis in the BALB/cJ mouse, that may depend on specific microanatomy or the quadruped nature of the mouse, is only a surrogate for human ONFH. The doses of LLP2A-Ale and PTH (1–34) were chosen from other pre-clinical studies that evaluated GC-induced bone loss and fracture healing (Guan et al., 2012; Yao et al., 2013; Mohan et al., 2017; Yao et al., 2016a). The optimal dosing regimen for LLP2A-Ale or PTH (1–34) in ON treatment may differ from one that shows bone efficacy. Given the finding of ON in a Control mouse, we recommend using a Control group as large as any treatment group. Unlike others who used four week old juvenile Balb/cJ mice as a model of ON, we used eight week old young adult male Balb/cJ mice as a model of adult onset ONFH, perhaps leading to lower ON prevalence in our GC-only mice than is seen when treatment is begun at age four weeks. Our results should not be generalized to younger mice or children. We performed immunohistochemistry to determine the presence of blood vessels within the DFE. However we did not evaluate mRNA from the bone samples to confirm that these proteins were being produced by either the bone or endothelial cells.

In summary, the prevalence of ON was higher in GC-treated mice than in control mice, and neither LLP2A-Ale nor hPTH (1–34) significantly affected the prevalence of GC-induced ON in this mouse model. The bone effects of LLP2A-Ale and hPTH (1–34) previously observed in Swiss Webster mice (Mohan et al., 2017) were confirmed in Balb/cJ mice.

Acknowledgements

This work was funded by the California Institute of Regenerative Medicine (CIRM), and National Institutes of Health (NIH) grants Nos. R01 AR043052, 1K12HD05195801 and 5K24AR048841-09. Statistical support was made possible by grant No. UL1 RR024146 from the National Center for Research Resources (NCRR), a component of the NIH and NIH Roadmap for Medical Research.

Authors' roles

Study design: NEL, WY. Study conduct: GM, WY, NEL; Data collection: GM, WY, DBK, KS, JJ, AD. Data analysis: GM, WY, NEL, DBK. Data interpretation: NEL, WY, DBK. Drafting manuscript: NEL, WY. Revising manuscript content: NEL, WY, DBK. Approving final version of manuscript: NEL, GM, WY, KS, YEL, JJ, AD, DBK. NEL takes responsibility for the integrity of the data analysis.

Conflict of interest

None.

References

Bednarek, A., Atras, A., Gagala, J., Kozak, L., 2010. Operative technique and results of core decompression and filling with bone grafts in the treatment of osteonecrosis of femoral head. Ortop. Traumatol. Rehabil. 12, 511–518.

Bouamar, R., Koper, J.W., et al., 2009. Polymorphisms of the glucocorticoid receptor and avascular necrosis of the femoral heads after treatment with corticosteroids. NDT Plus 2, 384–386. https://doi.org/10.1093/ndtPlus/sfp082.

Bouxsein, M.L., et al., 2010. Guidelines for assessment of bone microstructure in rodents using micro-computed tomography. J. Bone Min. Res. 25, 1468–1486.

Camp, J.F., Colwell, C.W., 1986. Core decompression of the femoral head for osteonecrosis. J. Bone Joint Surg. Am. 68, 1313–1319.

Cao, L., Guo, C., Chen, J., Chen, Z., Yan, Z., 2017. Free vascularized fibular grafting improves vascularity compared with core decompression in femoral head osteonecrosis: a randomized clinical trial. Clin. Orthop. Relat. Res. 475, 2230–2240. https://doi.org/10.1007/s11999-017-5374-x.

Chan, K.L., Mok, C.C., 2012. Glucocorticoid-induced avascular bone necrosis: diagnosis and management. Open Orthop. J. 6, 449–457. https://doi.org/10.2174/1874325001206010449.

Chen, C.H., et al., 2012. Alendronate in the prevention of collapse of the femoral head in nontraumatic osteonecrosis: a two-year multicenter, prospective, randomized,

double-blind, placebo-controlled study. Arthritis Rheum. 64, 1572–1578. https://doi.org/10.1002/art.33498.
Classen, T., Warwas, S., Jager, M., Landgraeber, S., 2017. Two-year follow-up after advanced core decompression. J. Tissue Eng. Regen. Med. 11, 1308–1314. https://doi.org/10.1002/term.2056.
Cui, Q., Wang, G.J., Balian, G., 1997. Steroid-induced adipogenesis in a pluripotential cell line from bone marrow. J. Bone Joint Surg. Am. 79, 1054–1063.
Dempster, D.W., et al., 2013. Standardized nomenclature, symbols, and units for bone histomorphometry: a 2012 update of the report of the ASBMR Histomorphometry Nomenclature Committee. J. Bone Miner. Res. 28, 2–17. https://doi.org/10.1002/jbmr.1805.
Dilisio, M.F., 2014. Osteonecrosis following short-term, low-dose oral corticosteroids: a population-based study of 24 million patients. Orthopedics 37, e631–e636. https://doi.org/10.3928/01477447-20140626-54.
Dong, Y., Li, Y., Huang, C., Gao, K., Weng, X., 2015. Systemic application of teriparatide for steroid induced osteonecrosis in a rat model. BMC Musculoskelet. Disord. 16, 163. https://doi.org/10.1186/s12891-015-0589-z.
Glueck, C.J., Freiberg, R.A., Fontaine, R.N., Sieve-Smith, L., Wang, P., 2001. Anticoagulant therapy for osteonecrosis associated with heritable hypofibrinolysis and thrombophilia. Expert Opin. Investig. Drugs 10, 1309–1316. https://doi.org/10.1517/13543784.10.7.1309.
Guan, M., et al., 2012. Directing mesenchymal stem cells to bone to augment bone formation and increase bone mass. Nat. Med. 18, 456–462. https://doi.org/10.1038/nm.2665.
Ikemura, S., Yamamoto, T., Nishida, K., Motomura, G., Iwamoto, Y., 2010. Gender difference in the development of steroid-induced osteonecrosis in rabbits. Rheumatology (Oxford) 49, 1128–1132. https://doi.org/10.1093/rheumatology/keq044.
Janke, L.J., et al., 2013. Primary epiphyseal arteriopathy in a mouse model of steroid-induced osteonecrosis. Am. J. Pathol. 183, 19–25. https://doi.org/10.1016/j.ajpath.2013.03.004.
Kawedia, J.D., et al., 2012. Substrain-specific differences in survival and osteonecrosis incidence in a mouse model. Comp. Med. 62, 466–471.
Lai, K.A., et al., 2005. The use of alendronate to prevent early collapse of the femoral head in patients with nontraumatic osteonecrosis. A randomized clinical study. J. Bone Joint Surg. Am. 87, 2155–2159. https://doi.org/10.2106/JBJS.D.02959.
Lane, N.E., Yao, W., 2010. Glucocorticoid-induced bone fragility. Ann. N. Y. Acad. Sci. 1192, 81–83. https://doi.org/10.1111/j.1749-6632.2009.05228.x.
Liu, C., et al., 2016. Asparaginase potentiates glucocorticoid-induced osteonecrosis in a mouse model. PLoS ONE 11, e0151433. https://doi.org/10.1371/journal.pone.0151433.
Mohan, G., et al., 2017. A novel hybrid compound LLP2A-Ale both prevented and rescued the osteoporotic phenotype in a mouse model of glucocorticoid-induced osteoporosis. Calcif. Tissue Int. 100, 67–79. https://doi.org/10.1007/s00223-016-0195-6.
Neer, R.M., et al., 2001. Effect of parathyroid hormone (1-34) on fractures and bone mineral density in postmenopausal women with osteoporosis. N. Engl. J. Med. 344, 1434–1441. https://doi.org/10.1056/NEJM200105103441904.
Peng, L., et al., 2006. Combinatorial chemistry identifies high-affinity peptidomimetics against α4β1 integrin for in vivo tumor imaging. Nat. Chem. Biol. 2, 381–389. https://doi.org/10.1038/nchembio798.
Peng, J., et al., 2011. Micro-CT-based bone ceramic scaffolding and its performance after seeding with mesenchymal stem cells for repair of load-bearing bone defect in canine femoral head. J Biomed Mater Res B Appl Biomater 96, 316–325. https://doi.org/10.1002/jbm.b.31770.
Powell, C., Chang, C., Naguwa, S.M., Cheema, G., Gershwin, M.E., 2010. Steroid induced osteonecrosis: an analysis of steroid dosing risk. Autoimmun. Rev. 9, 721–743. https://doi.org/10.1016/j.autrev.2010.06.007.
Powell, C., Chang, C., Gershwin, M.E., 2011. Current concepts on the pathogenesis and natural history of steroid-induced osteonecrosis. Clin. Rev. Allergy Immunol. 41, 102–113. https://doi.org/10.1007/s12016-010-8217-z.
Saag, K.G., et al., 2007. Teriparatide or alendronate in glucocorticoid-induced osteoporosis. N. Engl. J. Med. 357, 2028–2039. https://doi.org/10.1056/NEJMoa071408.
Saag, K.G., et al., 2009. Effects of teriparatide versus alendronate for treating glucocorticoid-induced osteoporosis: thirty-six-month results of a randomized, double-blind, controlled trial. Arthritis Rheum. 60, 3346–3355. https://doi.org/10.1002/art.24879.
Sheng, H., et al., 2009. Functional perfusion MRI predicts later occurrence of steroid-associated osteonecrosis: an experimental study in rabbits. J. Orthop. Res. 27, 742–747. https://doi.org/10.1002/jor.20765.
Wang, G.J., Dughman, S.S., Reger, S.I., Stamp, W.G., 1985. The effect of core decompression on femoral head blood flow in steroid-induced avascular necrosis of the femoral head. J. Bone Joint Surg. Am. 67, 121–124.
Weinstein, R.S., 2010. Glucocorticoids, osteocytes, and skeletal fragility: the role of bone vascularity. Bone 46, 564–570. https://doi.org/10.1016/j.bone.2009.06.030.
Weinstein, R.S., 2012a. Glucocorticoid-induced osteoporosis and osteonecrosis. Endocrinol. Metab. Clin. N. Am. 41, 595–611. https://doi.org/10.1016/j.ecl.2012.04.004.
Weinstein, R.S., 2012b. Glucocorticoid-induced osteonecrosis. Endocrine 41, 183–190. https://doi.org/10.1007/s12020-011-9580-0.
Weinstein, R.S., Jilka, R.L., Parfitt, A.M., Manolagas, S.C., 1998. Inhibition of osteoblastogenesis and promotion of apoptosis of osteoblasts and osteocytes by glucocorticoids. Potential mechanisms of their deleterious effects on bone. J. Clin. Invest. 102, 274–282. https://doi.org/10.1172/JCI2799.
Weinstein, R.S., Jilka, R.L., Almeida, M., Roberson, P.K., Manolagas, S.C., 2010. Intermittent parathyroid hormone administration counteracts the adverse effects of glucocorticoids on osteoblast and osteocyte viability, bone formation, and strength in mice. Endocrinology 151, 2641–2649. https://doi.org/10.1210/en.2009-1488.
Weinstein, R.S., et al., 2017. The pathophysiological sequence of glucocorticoid-induced osteonecrosis of the femoral head in male mice. Endocrinology 158 (11), 3817–3831. https://doi.org/10.1210/en.2017-00662.
Xie, X.H., et al., 2012. Promotion of bone repair by implantation of cryopreserved bone marrow-derived mononuclear cells in a rabbit model of steroid-associated osteonecrosis. Arthritis Rheum. 64, 1562–1571. https://doi.org/10.1002/art.34525.
Yamaguchi, R., et al., 2012. Effects of an anti-platelet drug on the prevention of steroid-induced osteonecrosis in rabbits. Rheumatology (Oxford) 51, 789–793. https://doi.org/10.1093/rheumatology/ker197.
Yang, L., et al., 2009. A mouse model for glucocorticoid-induced osteonecrosis: effect of a steroid holiday. J. Orthop. Res. 27, 169–175. https://doi.org/10.1002/jor.20733.
Yao, W., Lane, N.E., 2015. Targeted delivery of mesenchymal stem cells to the bone. Bone 70, 62–65. https://doi.org/10.1016/j.bone.2014.07.026.
Yao, W., et al., 2008a. Glucocorticoid excess in mice results in early activation of osteoclastogenesis and adipogenesis and prolongd suppression of osteogenesis: a longitudinal study of gene expression in bone tissue from glucocorticoid-treated mice. Arthritis Rheum. 58, 1674–1686. https://doi.org/10.1002/art.23454.
Yao, W., et al., 2008b. Glucocorticoid-induced bone loss in mice can be reversed by the actions of parathyroid hormone and risedronate on different pathways for bone formation and mineralization. Arthritis Rheum. 58, 3485–3497. https://doi.org/10.1002/art.23954.
Yao, W., et al., 2013. Reversing bone loss by directing mesenchymal stem cells to bone. Stem Cells 31, 2003–2014. https://doi.org/10.1002/stem.1461.
Yao, W., et al., 2016a. Improved mobilization of exogenous mesenchymal stem cells to bone for fracture healing and sex difference. Stem Cells 34, 2587–2600. https://doi.org/10.1002/stem.2433.
Yao, W., et al., 2016b. Sclerostin-antibody treatment of glucocorticoid-induced osteoporosis maintained bone mass and strength. Osteoporos. Int. 27, 283–294. https://doi.org/10.1007/s00198-015-3308-6.
Zalavras, C.G., Lieberman, J.R., 2014. Osteonecrosis of the femoral head: evaluation and treatment. J. Am. Acad. Orthop. Surg. 22, 455–464. https://doi.org/10.5435/JAAOS-22-07-455.
Zhang, H., et al., 2017. Acceleration of fracture healing by overexpression of basic fibroblast growth factor in the mesenchymal stromal cells. Stem Cells Transl. Med. https://doi.org/10.1002/sctm.17-0039.
Zhao, D., et al., 2012. Treatment of early stage osteonecrosis of the femoral head with autologous implantation of bone marrow-derived and cultured mesenchymal stem cells. Bone 50, 325–330. https://doi.org/10.1016/j.bone.2011.11.002.
Zhao, F.C., Guo, K.J., Li, Z.R., 2013. Osteonecrosis of the femoral head in SARS patients: seven years later. Eur. J. Orthop. Surg. Traumatol. 23, 671–677. https://doi.org/10.1007/s00590-012-1054-4.
Zhou, C.H., et al., 2017. PTH[1-34] improves the effects of core decompression in early-stage steroid-associated osteonecrosis model by enhancing bone repair and revascularization. PLoS ONE 12, e0178781. https://doi.org/10.1371/journal.pone.0178781.